Study of tungsten oxide and sulfate interactions on doubly-doped zirconia aerogels

Raymond A. Boyse and Edmond I. Ko*

Department of Chemical Engineering, Carnegie Mellon University, Pittsburgh, PA 15213-3890, USA
E-mail: edko@cmu.edu

Received 27 June 1997; accepted 19 September 1997

A zirconia aerogel, prepared by a sol–gel route followed by supercritical drying, was doped with both tungstate and sulfate by sequential incipient wetness impregnations. The role of the dopants and activation temperature on the physical and chemical properties was studied. The materials were characterized by nitrogen adsorption, X-ray diffraction, *n*-butane isomerization, Raman and infrared spectroscopy. Tungstate and sulfate were catalytically active over non-overlapping ranges of activation temperature and thus offered no synergistic catalytic effects. The effects of the two dopants on each other appeared to be primarily physical.

Keywords: zirconia, tungsten oxide, sulfate, aerogel, butane

1. Introduction

Acid catalysis plays a key role in many hydrocarbon conversion reactions of the chemical and petroleum industries [1]. The potential for an environmentally benign heterogeneous catalyst has driven the ongoing research of materials as substitutes for current liquid acids or halogen based solid acids [2]. Among these is the emerging class of catalytic materials of oxides modified by anionic or oxide dopants. The work of Hino et al. on sulfated [3] and tungstated [4,5] zirconias has initiated extensive research on these materials because of their activity in the skeletal isomerization of *n*-butane, a reaction of interest for the production of octane-enhancers to gasoline. The promise of these materials has been illustrated by several recent developments: Fe and Mn promoted sulfated zirconia exhibits extremely high activity at low temperatures in the isomerization of low alkanes [6]; Pt promoted tungstated zirconia shows superior selectivity in isomerizations of larger alkanes such as *n*-heptane [7].

These developments encourage the study of other sets of dopants – one such combination is that of zirconia promoted with both tungstate and sulfate. Huang et al. probed this material using the Hammett indicator method to show that the dopants have a synergistic effect on the resulting acid strength [8]. No catalytic data were available to support this conclusion. Miao et al. also compared zirconia–tungstate–sulfate to a set of doped zirconias and showed its catalytic activity in *n*-butane isomerization was less than that of zirconia–sulfate [9]. It is noted that the materials of Miao et al. were calcined at different temperatures to those of Huang et al. Therefore, it is not yet possible to ascertain if doping zirconia with sulfate and tungstate has a synergistic or detrimental catalytic effect.

Considerable information is presently available on the individual sulfated zirconia [10–13] and tungstated zirconia [7,14–16] materials. Sulfated zirconia is reported as highly active after calcination around 898 K due to enhanced surface acidity caused by the electron inductive effect of S=O double bonds in the surface sulfate. The exact nature of the active site and the corresponding acidity, although still unclear, are believed to be a function of water content and hence the preparative history of the material. Tungstated zirconia is reported as catalytically active in *n*-butane isomerization after calcination in the range 1073 to 1123 K [4,14]. Optimum calcination temperature enables solid–solid wetting of zirconia by tungstate to saturation monolayer coverage [7]. Cited advantages of tungstate, over sulfate, include the absence of dopant loss during thermal treatment and resistance to deactivation during catalytic reaction [14–16].

The aim of this work is to explore the effect of doubly-doping zirconia with sulfate and tungstate and investigate any synergy between the dopants. The individual materials, zirconia–sulfate and zirconia–tungstate, have been previously prepared and characterized in our laboratory [14,17]. Consequently, zirconia–tungstate–sulfate aerogel can be compared to materials with very similar preparative histories, thus reducing the variables that can inadvertently alter chemical properties. We used dopant loadings similar to those of the previously prepared aerogels to afford meaningful comparisons of catalytic and acidic data. This approach allowed us to gain an understanding of the interaction between an

* To whom correspondence should be addressed.

anionic and an oxide dopant, and its effect on the chemical properties of zirconia.

2. Experimental

2.1. Sample preparation

A zirconia–tungstate–sulfate aerogel was prepared by the sequential impregnations to incipient wetness of a zirconia aerogel by tungstate and sulfate. An undoped zirconia aerogel support was prepared by the sol–gel method followed by supercritical drying with CO_2 which has been described elsewhere [18]. Briefly, we added 16.2 ml zirconium *n*-propoxide (70 wt% in propanol, Alfa) to a solution of 15 ml 1-propanol (Fisher) and 1.91 ml HNO_3 (70% w/w, Fisher). In a second beaker, 1.31 ml distilled water was mixed with 15 ml 1-propanol. The contents of the second beaker were added to the contents of the first which was stirred until gelation occurred. The product alcogel was aged for 2 h at room temperature before displacement of the alcohol solvent by carbon dioxide under supercritical conditions in an autoclave [18]. The product aerogel was ground into a powder to pass through 100 mesh. Subsequent drying consisted of heating at 383 K under a vacuum for 3 h to remove water, followed by heating at 523 K under vacuum for 3 h to remove residual nitrates (from nitric acid used in the preparation). The X-ray amorphous powder was impregnated to incipient wetness with an aqueous solution of ammonium metatungstate hydrate (Aldrich) to yield a sample with a nominal loading of 10 wt% W. The product was again dried under vacuum at 383 and 523 K for 3 h. Sulfate was added by incipient wetness impregnation with an aqueous solution of ammonium sulfate to produce a material with a nominal sulfate loading of 10 mol% SO_4. The loadings of tungstate and sulfate were chosen to allow comparison with previous singly-doped samples studied in our laboratory. The sample underwent vacuum drying at 383 K followed by calcination to 773 K for 2 h in flowing O_2. The doubly-doped aerogel was finally activated by calcination in O_2 for 2 h at a temperature in the range 848–1223 K. We designated this material as $Z/WO_x/SO_x$.

The doubly-doped material was compared to two singly-doped materials: zirconia–tungstate [14] and zirconia–sulfate aerogels [17]. Characterization of zirconia–sulfate was also performed in this work to enable comparison, under identical conditions, to the doubly-doped aerogel. The data referred to in this work on zirconia–tungstate have been published elsewhere unless otherwise noted [14]. Briefly, undoped zirconia aerogel supports were prepared as described above. After the 523 K drying treatment, the supports were impregnated to incipient wetness by aqueous solutions of ammonium metatungstate and ammonium sulfate to yield zirconia–tungstate and zirconia–sulfate aerogels with 10 wt% (6.9 mol%) W and 10 mol% (8.0 wt%) SO_4, respectively. Zirconia–tungstate was vacuum dried at 383 K for 3 h and calcined in O_2 for 2 h in the range 1073–1223 K. Zirconia–sulfate was vacuum dried at 383 K and calcined in O_2 for 2 h at 773 K before activation by calcination in the range 848–1023 K. The singly-doped aerogels were designated as Z/WO_x and Z/SO_x.

2.2. Sample characterization

Textural characterization was determined by nitrogen adsorption/desorption using an Autosorb-1 gas sorption system (Quantachrome Corp.). Samples were outgassed at 383 K, under vacuum, for 2 h prior to analysis. Forty point desorption isotherms were obtained, from which the BET surface area, total pore volume, and pore size distribution were calculated. Crystal phases were identified from X-ray powder diffraction (XRD) patterns obtained using a Rigaku D/max diffractometer with Cu K_α radiation. Laser Raman spectra were recorded using a Spex 1403 0.85 m double spectrometer. The 488 nm line of a Spectra-Physics model 2020 argon ion laser, with a power output of about 200 mW, was used for excitation. Spectra were gathered from stationary samples contained in glass vials, under ambient conditions, over the range 200–1100 cm^{-1} with a spectral slit width of 600 μm and a step size of 2 cm^{-1}. The most prominent Raman bands are from the W–O vibrations of crystalline WO_3 at about 805 and 710 cm^{-1} by which the crystallization of tungsten oxide was monitored [19].

Catalytic activities were determined using a differential, downward flow, tubular fixed bed reactor operated at atmospheric pressure. Approximately 0.5 g of sample was pretreated at 588 K for 1 h under 2.4 ℓ/h (40 sccm) flowing helium. The sample was then cooled to 553 K and exposed to a feed stream mixture of 0.06 ℓ/h (1 sccm) *n*-butane (Matheson, Research Grade) in 0.60 ℓ/h (10 sccm) hydrogen (Matheson UHP). A Gow-Mac 550P gas chromatograph with thermal conductivity detector (Column: Supelco 23% SP 1700 on 80/20 Chromosorb, 1/8 in $\times$30 ft) was used to determine the composition of the product stream.

Diffuse reflectance infrared Fourier transform (DRIFT) spectroscopy was employed to characterize the surface acidity using a Mattson Galaxy 5020 FTIR, with a DTGS detector and a Harrick diffuse reflectance attachment (DRA-2). In situ DRIFT spectroscopy was performed using a Harrick reaction chamber (HVC-DR2). Each spectrum was obtained by averaging 128 scans taken over the range 400–4000 cm^{-1} at a resolution of 2 cm^{-1}. Ex situ and in situ DRIFT spectra were obtained from samples diluted to 5 wt% in KBr. Ex situ spectra were acquired under ambient conditions, while in situ DRIFT spectra were acquired under flowing helium at about 2.4 ℓ/h after pretreatment at 588 K for 15 min, the same pretreatment temperature to that used in the isomerization of *n*-butane. To measure the type

and strength of acidity on the surface, the samples were cooled to 373 K and subsequently exposed to pyridine for 15 min by diverting the helium flow through a pyridine saturator. Spectra were then taken at 373, 423, 473, 553 and 623 K after 5 min in flowing helium at each temperature. The type of surface acidity was determined by the peaks of adsorbed pyridine at 1445 and 1490 cm^{-1}. The former peak is caused by the presence of coordinately bound pyridine on Lewis acid sites and the latter by pyridine irreversibly adsorbed on both Brønsted and Lewis acid sites [20]. Relative amounts of Brønsted and Lewis sites were calculated using the integrated peak areas at 1445 and 1490 cm^{-1} [21]. The percentages of Brønsted acid sites were estimated on samples heated at 473 K. The relative strength of the acid sites was determined by monitoring the effect of temperature on the peaks at 1445 and 1490 cm^{-1}. Materials with stronger Brønsted acid sites retained irreversibly adsorbed pyridine up to higher temperatures.

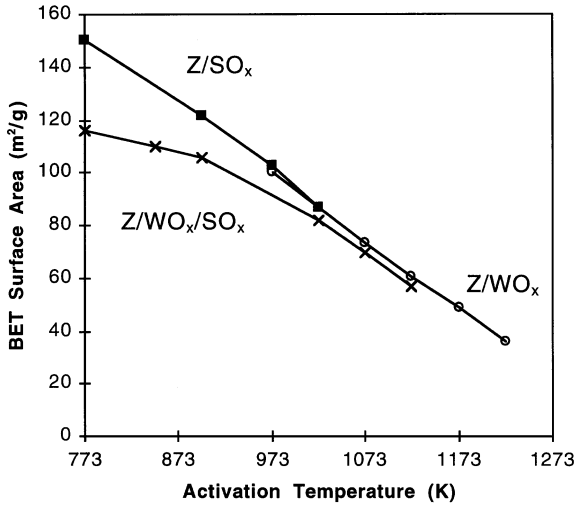

Figure 1. Effect of heat treatment (calcination at indicated temperature for 2 h) on the BET surface areas for zirconia aerogel promoted with tungstate (Z/WO_x), sulfate (Z/SO_x), and tungstate–sulfate ($Z/WO_x/SO_x$).

3. Results

3.1. Textural and structural properties

The BET surface areas and pore volumes of zirconia–tungstate–sulfate aerogels, activated at a range of temperatures, are given in table 1. After calcination at 773 K, the sample had a surface area of 116 m^2/g which is approximately that of a zirconia aerogel calcined at the same temperature [18]. Activation at 1073 K produced a material with 70 m^2/g which approximates that of a zirconia–tungstate aerogel with a surface area of 73 m^2/g [14]. Figure 1 illustrates the effect of activation temperature on the surface areas of $Z/WO_x/SO_x$, Z/SO_x, and Z/WO_x samples. The textural properties of zirconia–tungstate–sulfate appeared to be identical to those of zirconia–tungstate. The pore volumes and pore size distributions were similar to those of previously prepared zirconia aerogels [18].

The crystal phases of the samples were determined using X-ray diffraction and Raman spectroscopy. Table 1 shows that $Z/WO_x/SO_x$ was X-ray amorphous after activation at 773 K, then crystallized into the tetragonal phase of zirconia in the range 848–898 K, and began to transform into the monoclinic phase after activation at 1223 K. Raman spectra of the same samples allowed the crystallization of WO_3 on the surface of zirconia to be monitored. Figure 2 compares the Raman spectra of $Z/WO_x/SO_x$ and Z/WO_x at 1073 and 1123 K. Crystalline

Table 1
Physical properties of zirconia–tungstate–sulfate ($Z/WO_x/SO_x$) aerogels

Calcination temperature (K)	Surface area (m^2/g)	Pore volume (cm^3/g)	Crystalline structure of ZrO_2 [a]	WO_3 nominal loading [b] (W-atoms/nm^2)
773	116	0.29	A	3.14
848	110	0.29	A/T	3.31
898	105	0.29	T	3.47
1023	82	0.28	T	4.44
1073	70	0.28	T	5.20
1123	57	0.26	T	6.39
1223	26	0.15	T / M	14.00

[a] Determined by X-ray powder diffraction: A - amorphous; T - tetragonal; M - monoclinic.

[b] Calculation based on the experimentally determined BET surface areas and assuming each W-unit occupied a surface area of 0.16 nm^2.

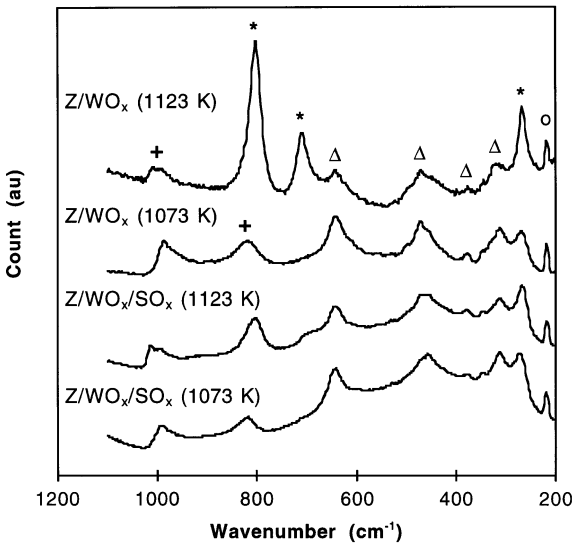

Figure 2. Raman spectra for the zirconia–tungstate (Z/WO_x) and zirconia–tungstate–sulfate ($Z/WO_x/SO_x$) aerogels after calcination at 1073 and 1123 K. Peak indices: (*) crystalline WO_3; (△) ZrO_2; (+) surface tungstate; (○) plasma line.

WO_3 was evident on Z/WO_x after calcination at 1123 K by Raman bands, caused by W–O vibrations, at 802 and 710 cm^{-1}. At a lower calcination temperature of 1073 K, a weak peak was evident at 820 cm^{-1} but not at 710 cm^{-1}. We assigned the peak at 820 cm^{-1} to the W–O–W vibration of surface tungstate [19] because the W–O vibration of crystalline WO_3 at 710 cm^{-1} was absent. Hence, crystalline WO_3 was detectable at 1123 K, but not at 1073 K. The Raman spectra of $Z/WO_x/SO_x$ detected the presence of a small amount of WO_3 after calcination at 1123 K, as evidenced by a weak peak at 710 cm^{-1}. After calcination at 1073 K, the presence of a peak at 820 cm^{-1}, and absence of a peak at 710 cm^{-1}, indicated that tungstate remained in a dispersed state up to this temperature. In sum, activation at 1123 K caused substantially more crystallization of WO_3 on Z/WO_x than on $Z/WO_x/SO_x$ as illustrated by the larger Raman peaks at 802 and 710 cm^{-1}.

The existence and nature of sulfate on $Z/WO_x/SO_x$ samples were determined using DRIFT spectroscopy and thermogravimetric analysis (TGA). TGA curves, shown as a derivative of weight (rate of loss) versus temperature, of the singly- and doubly-doped aerogels are compared in figure 3. A rapid weight loss occurred in the range 873–1073 K from all of the aerogels. This loss, also present on zirconia–tungstate, was attributed to the loss of residual organic or hydroxyl species upon crystallization of ZrO_2. The weight loss from Z/SO_x was significantly larger and was associated with the decomposition of sulfate during support crystallization [17]. A smaller continuous loss was observed from 973 to 1223 K also due to sulfate loss with increasing temperature. The TGA curve in figure 3 for $Z/WO_x/SO_x$ exhibited near identical behavior to Z/SO_x but the peaks occurred at a higher temperature, illustrated by the peak maxima at 1010 and 938 K, respectively. Therefore, even though sulfate decomposed from $Z/WO_x/SO_x$ in a manner similar to Z/SO_x, the higher temperature of decomposition indicated a delay in the crystallization of ZrO_2 and hence a further stabilization of ZrO_2 by two dopants.

DRIFT spectroscopy was used to examine the effect of calcination temperature on sulfate, and probe for interactions between sulfate and tungstate. Figure 4 shows the ex situ DRIFT spectra of $Z/WO_x/SO_x$ in the range 900–1500 cm^{-1}. All of the samples calcined in the range 773–898 K displayed broad infrared bands around 1050, 1140 and 1230 cm^{-1} verifying the existence of sulfate on ZrO_2. Peak shifts were observed with increasing calcination temperature, in particular a peak shift from 1230 to 1250 cm^{-1} with calcination from 848 to 898 K. Previous work has associated this peak with an S=O vibration, and the shift in peak position to the transition of surface sulfate into a catalytically active species [17]. At 1023 K and above, no sulfate infrared vibrations were evident demonstrating there was no sulfate remaining on these $Z/WO_x/SO_x$ samples. Finally, a peak at 960–980 cm^{-1} established that tungstate species were present on the zirconia support [14]. No new vibrations due to sulfate–tungstate interactions were observed.

3.2. Catalytic and acidic properties

The catalytic properties of the $Z/WO_x/SO_x$ samples were examined using the isomerization of *n*-butane in H_2 at 553 K. Figure 5 shows the catalytic activities of representative samples with time-on-stream. $Z/WO_x/SO_x$ calcined at 898 K showed a noticeable decline in catalytic activity with time-on-stream which was the case with all the samples calcined below 1023 K. $Z/WO_x/SO_x$ calcined at 1123 K maintained a relatively constant activity similar to samples calcined at 1023 K and above. Singly-doped aerogels, Z/WO_x and Z/SO_x, after activation at 1123 and 898 K, respectively, showed higher activities

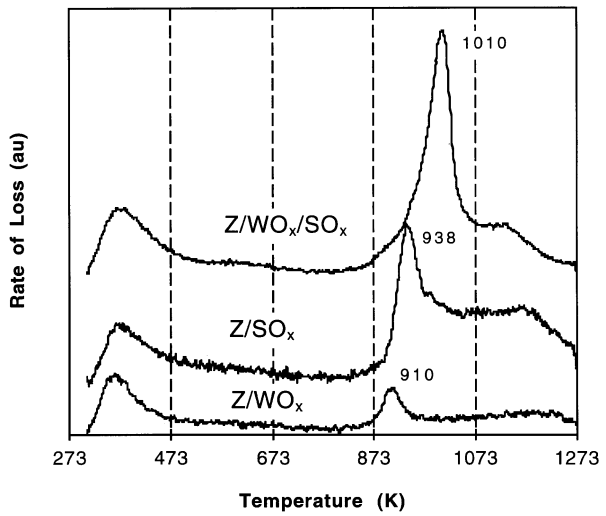

Figure 3. Thermogravimetric analysis (TGA) of zirconia aerogels promoted with tungstate (Z/WO_x), sulfate (Z/SO_x), and tungstate–sulfate ($Z/WO_x/SO_x$). Samples were calcined for 2 h at 773 K in O_2.

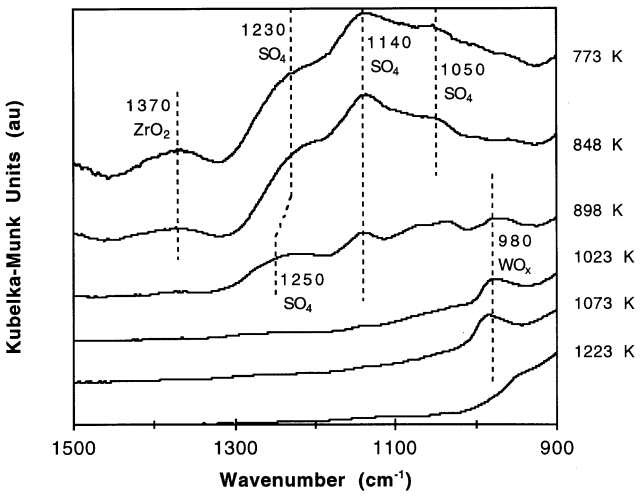

Figure 4. Ex situ DRIFT spectra for zirconia–tungstate–sulfate ($Z/WO_x/SO_x$) aerogel over a range of activation temperatures.

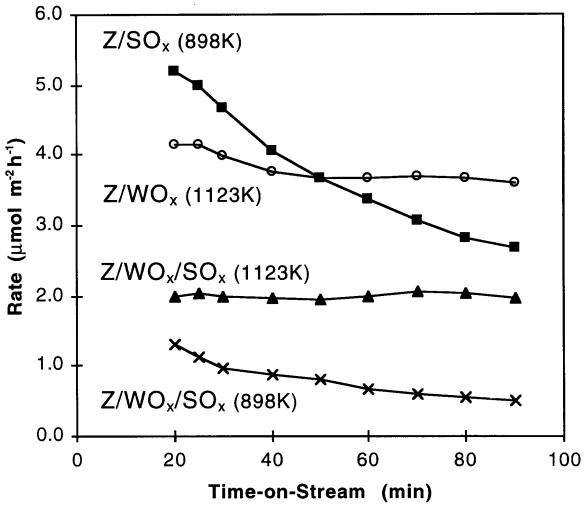

Figure 5. Catalytic activity of selected aerogels in *n*-butane isomerization at 553 K in H_2 after pretreatment at 588 K for 1 h in He.

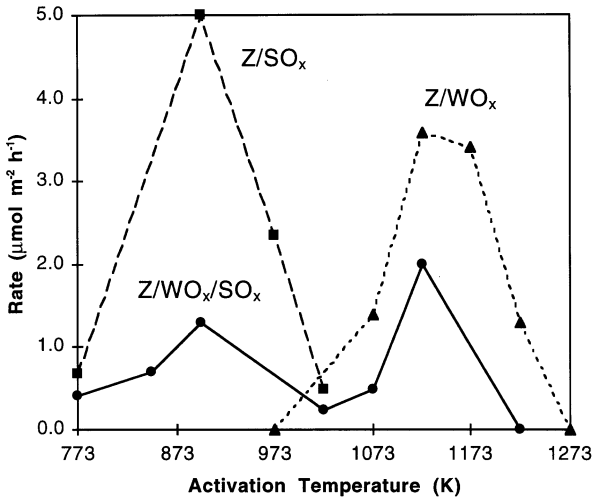

Figure 7. Effect of activation temperature on the initial activity (20 min time-on-stream) in *n*-butane isomerization at 553 K in H_2 for zirconia–tungstate–sulfate ($Z/WO_x/SO_x$), zirconia–tungstate (Z/WO_x) and zirconia–sulfate (Z/SO_x) aerogels.

while Z/WO_x exhibited less deactivation with time-on-stream than Z/SO_x. Figure 6 displays the effect of activation temperature on the initial and final activities of the doubly-doped aerogel. As mentioned, the final activity was significantly less than the initial activity when the calcination temperature was less than 1023 K. Two calcination temperatures generated materials that were noticeably active in the isomerization of *n*-butane: 898 and 1123 K. Figure 7 compares the activity profile of $Z/WO_x/SO_x$ to those of Z/WO_x, which has been reported elsewhere [14], and Z/SO_x which was determined in this work. Z/SO_x was catalytically active in the range 773–1023 K and Z/WO_x was active in the range 973–1223 K. We observed that the two temperatures of high activity on $Z/WO_x/SO_x$ matched the optimum calcination temperatures for singly-doped zirconia–sulfate and zirconia–tungstate aerogels with 10 mol% SO_4 and 10 wt% W, respectively.

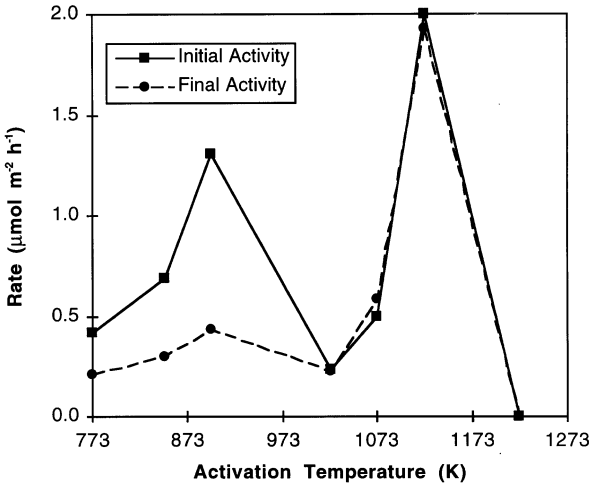

Figure 6. Effect of activation temperature on the initial activity (20 min time-on-stream) and steady-state activity (90 min time-on-stream) in *n*-butane isomerization at 553 K in H_2 for zirconia–tungstate–sulfate ($Z/WO_x/SO_x$) aerogel.

The surface acidity of the most active $Z/WO_x/SO_x$, calcined at 898 and 1123 K, was examined using DRIFT spectroscopy of adsorbed pyridine. The properties were compared to the singly-doped zirconia–tungstate and zirconia–sulfate aerogels and can be found in table 2. All the samples showed evidence of Brønsted and Lewis acidity by peaks at 1540, 1490 and 1445 cm^{-1}. The relative amounts of Brønsted sites at 473 K, given in table 2, varied from approximately 20% on $Z/WO_x/SO_x$ calcined at 898 K to 55% on Z/WO_x calcined at 1123 K. The temperature range at which pyridine desorbed from the Brønsted sites is given in table 2 and indicated the relative strength of the sites. $Z/WO_x/SO_x$ calcined at 898 K exhibited no pyridine vibrations on Brønsted acid sites at 553 K in helium suggesting that the acidity of this sample was weaker than that of the other samples. DRIFT spectra of Z/SO_x calcined at 898 K showed the presence of adsorbed pyridine above 623 K indicating that this sample possessed the strongest Brønsted acid sites of all the samples.

4. Discussion

Results in this study allowed us to understand the type and extent of interactions between tungstate and sulfate on zirconia as well as how these interactions affect the physical and chemical properties of the aerogel. As described above, two activation temperatures produced a doubly-doped aerogel that had a high catalytic activity: 898 and 1123 K. By comparison to the activity profiles of Z/WO_x and Z/SO_x in figure 7, it was clear that these two temperatures matched the optimum activation

Table 2
Catalytic and acidic properties of selected aerogels

Sample	Calcination temperature (K)	*n*-butane isomerization activity [a] (μmol/(h m^2))	%Brønsted acid sites of total acid sites at 473 K [b]	Temperature range of pyridine desorption from Brønsted acid sites [c] (K)
$Z/WO_x/SO_x$	898	1.30/0.44	20	473–553
$Z/WO_x/SO_x$	1123	2.03/1.93	40	553–623
Z/SO_x	898	5.20/2.69	46	623–673
Z/WO_x	1123	4.15/3.59	55	553–623

[a] Initial and final activities after 20 and 90 min time-on-stream, respectively.
[b] Determined by FT-IR spectroscopy of irreversibly adsorbed pyridine, given with approximately ±5% accuracy.
[c] Determined by pyridine FT-IR spectroscopy.

temperatures of the singly-doped aerogels. We also observed that the activity profile of $Z/WO_x/SO_x$ was qualitatively similar to a combination of the activity profiles of Z/SO_x and Z/WO_x from 773–898 K and 1023–1223 K, respectively.

In the lower temperature range, DRIFT spectroscopy confirmed the presence of sulfate and tungstate on the surface of $Z/WO_x/SO_x$. The infrared peak shift from 1230 to 1250 cm^{-1} suggested that the population of catalytically active surface sulfate increased as the calcination temperature increased from 773 to 898 K [17]. The increasing amount of active sulfate was reflected in the increasing initial catalytic activities shown in figure 6. Note in figure 7, however, that the specific activity of $Z/WO_x/SO_x$ was significantly lower than that of Z/SO_x, suggesting that the presence of tungstate adversely affected the catalytic activity. As shown in table 1, the tungstate loading in $Z/WO_x/SO_x$ corresponded to 3.14–3.47 W-atoms/nm^2, or approximately 0.5–0.6 theoretical monolayers over this temperature range. Thus, a large portion of the surface was covered by tungstate, making it less likely to find adjacent sulfate and hydroxyl groups which are necessary to generate strong acidity [17]. In essence, surface tungstate reduced the effective sites available for reaction and, in turn, the specific catalytic activity. Data in table 2 show that for the samples activated at 898 K, $Z/WO_x/SO_x$ did possess proportionally less and weaker Brønsted acid sites than Z/SO_x, in support of the above model accounting for the effect of surface tungstate. This model is also consistent with the results of Miao et al. who observed a decrease in catalytic activity after adding tungstate to sulfated zirconia [9].

In the higher calcination temperature range of 1023–1223 K, the $Z/WO_x/SO_x$ sample exhibited a constant activity in *n*-butane isomerization with time-on-stream, similar to previous results for zirconia–tungstate [14]. The highest catalytic activity occurred at 1123 K for both $Z/WO_x/SO_x$ and Z/WO_x. Recall that DRIFT spectra (see figure 4) showed that sulfate was no longer present on the surface of $Z/WO_x/SO_x$ at 1023 K and above, verifying that tungstate was the remaining dopant in this temperature range. Thus, it is not surprising that $Z/WO_x/SO_x$ and Z/WO_x exhibited very similar activation behavior. What is not immediately obvious is why the former showed a lower specific catalytic activity. After all, these two samples had very similar acidic properties. Comparison of $Z/WO_x/SO_x$ and Z/WO_x calcined at 1123 K, shown in table 2, illustrated the similar *relative* amounts of Lewis and Brønsted acid sites – 40 and 55% Brønsted acidity, respectively. The strength of Brønsted acidity, determined by the highest temperature at which pyridine remained on the surface, also appeared to be the same for both samples.

We speculate that the lower activity of $Z/WO_x/SO_x$ was due to a less "mature" development of the active surface tungstate species. Apparently even though surface sulfate was no longer present at high activation temperatures, its influence was felt through its earlier effect on the crystallization of the zirconia support. TGA data in figure 3 showed that having both dopants, sulfate and tungstate, stabilized ZrO_2 against crystallization to higher temperatures than those samples containing either dopant alone (1010 K versus 938 and 910 K). This enhanced stability of the support means that the sintering and crystallization of surface tungstate proceeded to a lesser extent at the same activation temperature. Corroborative evidence of this model is the much smaller Raman peak at 802 cm^{-1} for $Z/WO_x/SO_x$ than for Z/WO_x after calcination at 1123 K, indicating much less crystalline WO_3 on the doubly-doped aerogel. Since the development of the active surface tungstate species and crystalline WO_3 take place simultaneously during activation of the sample [14], it stands to reason that the former was also less developed due to the delayed crystallization of the support. A lower density of the surface active species would explain the lower catalytic activity observed.

The essence of our finding is that there were two regimes of catalytic activity: between 773 and 898 K, sulfate was the active species; between 1023 and 1173 K, tungstate was the active species. The dopants enhanced the catalytic activity of zirconia independently because they had non-overlapping ranges of activation temperature. Their effects on each other were primarily physical – tungstate blocked the available surface for sulfate, while sulfate together with tungstate stabilized the sup-

Table 3
Effect of sulfate on optimally-calcined zirconia–tungstate aerogel

Sample	Calcination temperature (K)	Surface area (m^2/g)	*n*-butane isomerization activity [a] (μmol/(h m^2))
Z/WO_x	1123	54	4.15/3.59
Z/WO_x(1123 K)/SO_x	898	53	1.23/1.33
Z/SO_x	898	122	5.20/2.69

[a] Initial and final activities after 20 and 90 min time-on-stream, respectively.

port. The remaining question is: would sulfate and tungstate interact chemically if they are present on the support at the same time? As a first step to address this issue, we prepared another sample on which tungstate was activated *before* the addition and activation of sulfate. A zirconia–tungstate aerogel was activated by calcination to 1123 K, at which point saturation coverage of the surface of ZrO_2 by tungstate yielded a highly active material [7,14]. Then 10 mol% sulfate was added by incipient wetness impregnation and activated by calcination to 898 K. Table 3 compares the surface area and catalytic activity of this material to Z/WO_x and Z/SO_x. After activation at 1123 K, the activity of $Z/WO_x/SO_x$ was significantly less than Z/WO_x. The lower activity indicated that acid site generation by dispersed tungstate was impeded by sulfate. Hence, synergy between dopants in *n*-butane isomerization did not occur even when both dopants were present at the loadings used in this study, at least not for a sample in which sulfate was introduced onto a tungstate-saturated surface. Other variables, including loadings, sequence of introduction, and activation temperature, need to be examined further in order to fully understand any potential tungstate–sulfate interactions on zirconia.

5. Conclusions

Zirconia–tungstate–sulfate aerogels were active in the isomerization of *n*-butane after activation in the range 773 to 1123 K. Because sulfate and tungstate were catalytically active over non-overlapping ranges of activation temperature, two distinct regimes of catalytic activity were observed. Between 773 and 898 K, sulfate was the active species. Tungstate was present on the surface but was not catalytically active; its presence lowered the specific catalytic activity. Between 1023 and 1173 K, tungstate was the active species while sulfate was not present on the surface due to thermal decomposition. A decrease in activity indicated a reduction in the population of catalytically active sites which was ascribed to the delay in crystallization of zirconia caused by both dopants. These results demonstrated the importance of activation temperature as a key variable in understanding catalytic behavior.

Acknowledgement

This work is supported by the Division of Chemical Sciences, Office of Basic Energy Sciences, Office of Energy Research, US Department of Energy (grant DE-FG02-93ER14345).

References

[1] A. Baiker and J. Kijenski, Catal. Today 5 (1989) 1.
[2] K. Tanabe, M. Misono, Y. Ono and H. Hattori, *New Solid Acids and Bases* (Elsevier, Amsterdam, 1989).
[3] M. Hino, S. Kobayashi and K. Arata, J. Am. Chem. Soc. 101 (1979) 6439.
[4] M. Hino and K. Arata, J. Chem. Soc. Chem. Commun. (1987) 1259.
[5] M. Hino and K. Arata, *Proc. 9th Int. Congr. on Catalysis* (Chem. Inst. Canada, Ottawa, 1988) p. 1727.
[6] K.T. Wan, C.B. Khouw and M.E. Davis, J. Catal. 158 (1996) 199.
[7] E. Iglesia, D.G. Barton, S.L. Soled, S. Miseo, J.E. Baumgartner, W.E. Gates, G.A. Fuentes and G.D. Meitzner, *Proc. 11th Int. Congr. on Catalysis* (Elsevier, Amsterdam, 1996) p. 533.
[8] Y. Huang, Z.G. Zhang and W. Zhang, Rare Metals 11 (1992) 185.
[9] C. Miao, W. Hua, J. Chen and Z. Gao, Catal. Lett. 37 (1996) 187.
[10] K. Arata, Adv. Catal. 37 (1990) 165.
[11] X. Song and A. Sayari, Catal. Rev. Sci. Eng. 38 (1996) 329.
[12] D.A. Ward and E.I. Ko, J. Catal. 150 (1994) 18.
[13] F. Garin, D. Andriamasinoro, A. Abdulsamad and J. Sommer, J. Catal. 131 (1991) 199.
[14] R.A. Boyse and E.I. Ko, J. Catal., accepted.
[15] G. Larsen, E. Lotero and R.D. Parra, *Proc. 11th Int. Congr. on Catalysis* (Elsevier, Amsterdam, 1996) p. 543.
[16] G. Larsen and L.M. Petkovic, Appl. Catal. A 148 (1996) 155.
[17] D.A. Ward and I.E. Ko, J. Catal. 157 (1995) 321.
[18] D.A. Ward and E.I. Ko, Chem. Mater. 5 (1993) 956.
[19] D.S. Kim, M. Ostromecki and I.E. Wachs, J. Mol. Catal. A 106 (1996) 93.
[20] E.P. Parry, J. Catal. 2 (1963) 371.
[21] M.R. Basila and T.R. Kantner, J. Phys. Chem. 70 (1966) 1681.
[22] E.I. Ko, R. Bafrali, N.T. Nuhfer and N.J. Wagner, J. Catal. 95 (1985) 260.